Numerically based qualitative evaluation of GPR vertical and horizontal resolutions for reinforced concrete structures

Tahar Bachiri [1,*], *Mohammed* Hamdaoui[2], *Gamil* Alsharahi[2], *Mohammed* Bezzazi[1], and *Ahmed* Faize[2]

[1]Faculty of Sciences and Technology, Tangier 91001, Abdelmalek Essaadi University, Morocco
[2]Polydisiplinarly Faculty of Nador, Mohammed First University, Morocco

Abstract. The GPR is widely used for non-destructive evaluation of reinforced concrete structures. High resolution of detection is needed in order to differentiate between multiple targets present in the host medium. This article aims to numerically study the vertical and horizontal resolutions associated to detection of reinforcing bars buried in a structure made from concrete by means of GPR inspection. Use was made of open source software GprMax2D by considering the three work frequencies: 1GHz, 1.6GHz and 2GHz. The method of scanning is assumed to be according to B-scan protocol which was conducted along a profile traced on the surface of the inspected member. In situ measurements were made for a bridge pillar made of reinforced concrete by the MALÅ CX GPR system with a frequency centred on 1.6 GHz. The obtained results show that the GPR is effective in the examination of reinforced concrete structure and most of the steel bars can be detected. After making correction, the horizontal resolution predicted by a conventional formula was verified. However, the real vertical resolution imposes a minimum distance separating steel bars that is higher than that proposed in the literature. This is due to the high conductivity of steel bars that yields strong reflection of the signal at the first reached bars and which impedes significant secondary reflection from targets located below them.

1 Introduction

Ground Penetrating radar (GPR) is a device widely used in non-destructive evaluation of reinforced concrete (RC) structures. The principle is based on the emission of an electromagnetic pulse which is centred on frequency belonging to the band $10MHz$ to $4GHz$. The GPR transmitting antenna sends out the pulse into the inspected medium and is partially reflected when it reaches a target having dielectric properties that are different from those of the host medium. The reflected wave is recorded by means of a receiving antenna. The control unit of the GPR enables to process the single traces (A-scan) corresponding to fixed positions of antennas into a B-scan radargram.

This GPR device was judged suitable for the inspection of the sub-surfaces, particularly for the assessment of location of buried pipes in soils and rebars in RC structures. It was successful in monitoring cracks in bridges, roads, pavements and tunnels [1-5]. However, this non-destructive testing technique can involve some shortcomings affecting the stages of data collection, analysis and interpretation. Heterogeneities of the inspected medium may cause a complex reflection pattern which is difficult to understand. This is the case for example of soils containing high concentrations of rocks, gravel, and roots [6]. In the case of a RC structure, multiple steel bars are present and each one of them creates a trace on the radargram. But a given bar will be distinguishable only if the reflected signal is significant. So, a fundamental topic in GPR testing is how to improve the quality of acquired data by considering the best configuration and settings of the GPR device.

One of the most significant factors that should be dealt with in the planning of non-destructive studies based on the GPR is to characterise the horizontal and vertical resolutions that intervene in detection of targets. For appropriate collection of GPR data, radar antennas must be selected for each specific study. This includes in particular the best selection of the work frequency. The GPR's resolution capability is largely influenced by this choice.

The purpose of this work is to investigate numerically both vertical and horizontal resolutions in terms of the work frequency and target depth. Use is made of the GprMax2D software according to B-scan protocol. An example of In-situ GPR measurement is considered at first. Then, extensive simulations are performed in order to determine the practical resolution limits in horizontal and vertical directions. Direct examination of the obtained radargrams is done to determine detectability of steel bars buried in concrete while varying the horizontal or the vertical distance separating them. Discussion is performed about validity of some theoretical formulas that were presented in the literature for the prediction of GPR resolution.

* Corresponding author: *tbachiri@uae.ac.ma*

2 Materials and method

2.1 Theoretical background of GPR resolution

The vertical and horizontal resolutions have been estimated through various formulas that were proposed in the literature. Let us consider two reflection events from two adjacent targets which are located on the same vertical, see Fig.1. The reflections are sensed at the time instants t_1 and t_2. The vertical resolution Δv is defined as the minimal depth distance separating the two targets that could be distinguished on the GPR radargram [7- 8]. Separation of the traces will be possible if the time delay $\Delta\tau = |t_2 - t_1|$ exceeds half the pulse duration denoted τ_p. The vertical resolution is then estimated by:

$$\Delta v = \frac{c\tau_p}{2} \quad (1)$$

where c is the velocity of electromagnetic waves.

The horizontal resolution Δh is defined as the minimum distance separating two targets, which are located at the same depth from the inspected surface, such that the GPR can detect them separately. A lot of formulas have been proposed in the literature to estimate this resolution [9-12]. One can find among them the statement illustrated by Fig. 2 for which the horizontal resolution is taken to be the radius of antenna footprint. This latter can be expressed under the following form:

$$\Delta h = R_H = \frac{\lambda}{4} + \frac{d}{\sqrt{\varepsilon_r + 1}} \quad (2)$$

where $\lambda = c/f$ represents the wavelength for the given work frequency f, ε_r is the relative dielectric permittivity to depth d of the reflector surface and R_H the radius of antenna footprint at depth d, see Fig. 2.

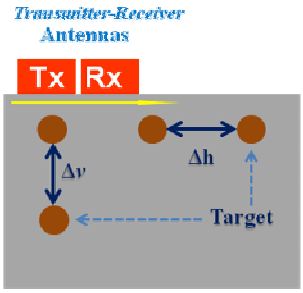

Fig. 1. Illustration of horizontal and vertical resolutions.

From Eqs. (1) and (2), one can see that the horizontal and vertical resolutions are strongly dependant on the work frequency. But, in practice the depth of penetration of the electromagnetic signal into the host medium is finite. This latter depends on the attenuation and writes

$$d_p = \frac{\lambda}{4\pi} \quad (3)$$

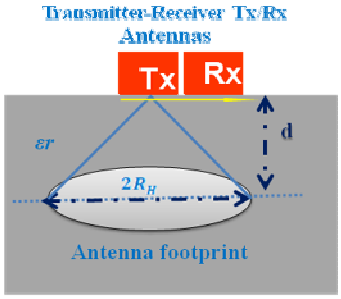

Fig. 2. Illustration of the antenna footprint in the host medium.

Eq. (3) states that the penetration depth is a small fraction of wavelength and decreases versus the GPR frequency. So there is a conflict resulting between decreasing horizontal and vertical resolutions on one hand and increasing the penetration depth on the other hand. A compromise should then be found in order to have sufficient amplitude of the GPR signal and desired resolutions. This depends on the host medium material.

2.2 A practical experiment

To have a clear idea about the practical issue of GPR resolution, a real GPR testing was carried out on a reinforced concrete bridge pillar having a diameter of $30cm$. Fig. 3 shows a photo of the pillar which was the subject of GPR testing. The figure indicates also the traces of the B-scans that were performed.

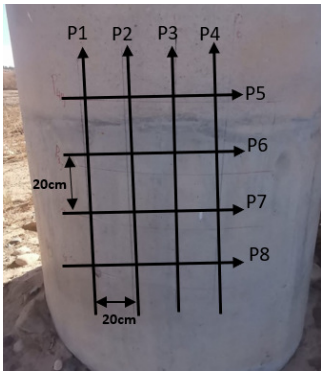

Fig. 3. Photo of the bridge pillar made of reinforced concrete that was tested by the GPR system MALÅ CX; the photo shows the traces along which B-scan was performed.

In the experiment, the GPR system MALÅ CX from the company MALA Geosciences was used. The work centre frequency was fixed at $1.6GHz$. The frequency bandwidth is delimited by $0.8GHz$ and $2.4GHz$. The time window was fixed at $9ns$. GPR surveys were conducted on an area of the bridge pillar of $60\times60cm$, where longitudinal and transverse B-scans were performed along the eight traces shown in Fig. 3.

Some of the collected radargrams are presented in Figs. 4 and 5. These correspond respectively to the horizontal line P7 and the vertical line P1 shown in Fig. 3. The pattern of reflection as obtained in the two radargrams shows the existence of ordered and repetitive hyperbolic signatures. Each signature is linked to a steel rebar. These hyperbolas are quite visible because of the

high contrast existing between the steel electric conductivity and that of concrete. Taking the first row of the hyperbolas, one can determine the depth of concrete cover. For the longitudinal B-scan conducted along the profile P1, the depth is about 3cm. Meanwhile for the transverse profile P7, the identified depth is around 5cm.

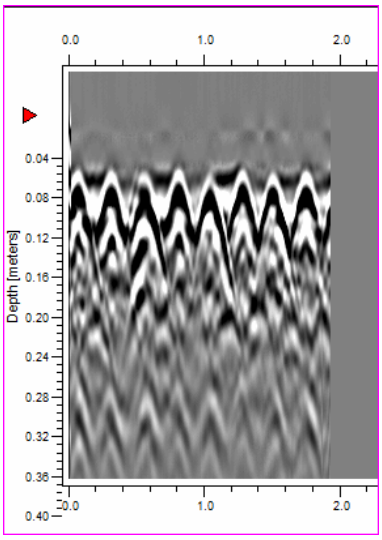

Fig. 4. Radargram for the transverse profile P7 as obtained from GPR system MALÅ CX.

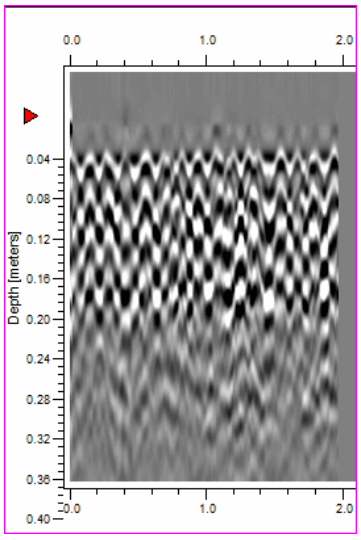

Fig. 5. Radargram for the longitudinal profile P1 as obtained from GPR system MALÅ CX.

Based on the radargram shown in Fig. 4, one can determine that the longitudinal rebars have a spacing of $30cm$. Fig. 5 shows that the transverse rebars have a spacing of about $15cm$. Horizontal resolution in this experiment enables to distinguish without problem between the adjacent steel bars of the first row along the two directions of inspection. Note that the radargrams become noisy and visibility of the traces is reduced after reaching a depth which is comprised between $16cm$ and $20cm$ for both of the profiles P1 and P7. This can be attributed to secondary reflections taking place at the rebars with high signal attenuation because of high steel conductivity.

To understand more deeply how vertical and horizontal resolution can change the radargram content, a case of study is simulated in the following.

2.3 Simulation of a case of study

In the following a concrete structure containing steel bars having the same diameter of $25mm$ is modelled by using GprMax2D software under Matlab environment [13]. GprMax2D software enables to simulate propagation of electromagnetic waves based on the finite difference in time domain method. The bars are located according to Fig. 6. The horizontal distance between the bars belonging to the second row is $5cm$, while the distance separating those of the third row is $10cm$. The first two rows are separated vertically by $5cm$, while the second and third rows are distant by $10cm$.

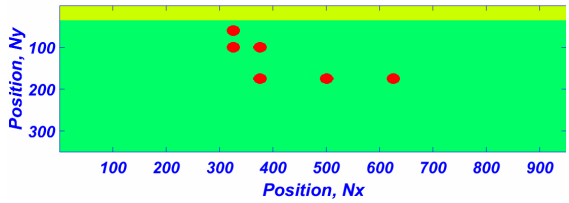

Fig. 6. Scheme of the simulated concrete structure containing steel bars.

Table 1 gives the materials properties used in GPR simulations. They consist of relative permittivity ε_r, relative permeability μ_r and electric conductivity σ. The calculated wave velocity c in m/ns is given in the last column of this table.

Table 1: Material parameters used in GPR simulation of the concrete domain shown in Fig. 6.

Material	ε_r	μ_r	$\sigma\,(S/m)$	$c\,(m/ns)$
Air	1	1	0	0.3
Concrete	6	1	0.0255	0.124
Steel	1.45	10^4	9.931×10^6	

GprMax2D enables to obtain a B-scan radargram along the top border of the concrete domain. Normally all targets should show a hyperbola trace which is associated to the reflected amplitude of wave on the steel bar. The expected number of hyperbolas is then 6. To assess this, the resolution is tested in the following for the three work frequencies $1GHz$, $1.6GHz$ and $2GHz$.

3 Results and discussion

3.1 Horizontal resolution

To study the outcome of simulation in terms of horizontal resolution, reference is made to Eq. (2) in

which a new parameter α reflecting geometric attenuation is introduced [14-16]. The horizontal resolution is considered under the following form [15]:

$$\Delta h = \frac{R_H}{1+\alpha} \quad (4)$$

In the present work, it is proposed to define the coefficient α as the ratio of the reflected signal amplitude from a bar located at the depth of $20cm$ divided by the reflected signal amplitude from the bar situated at the depth of $5cm$.

Fig. 7 gives the obtained radargram for the work frequency $f_2 = 1.6GHz$. From this figure, one can see that it is quite possible to distinguish between the hyperbolas associated to steel bars placed on the first, second and third rows, and presenting an eccentricity with regards to the first column. One can conclude then that the horizontal interval distances of Fig. 6 are within the margin of horizontal resolution.

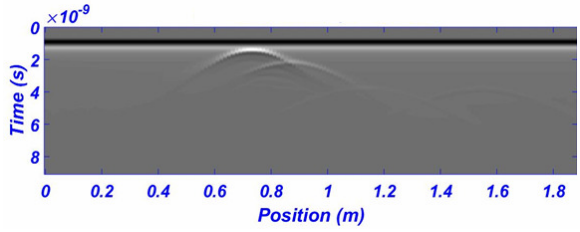

Fig. 7. B-scan radargram obtained with the work frequency $f_2 = 1.6GHz$ for the concrete structure shown in Fig. 6.

Post-treatment of a B-scan radargram, such as that given in Fig. 7, can be performed under Matlab in order to identify the reflection amplitudes from steel bars. Table 2 gives the obtained numerical results in terms of signal amplitude reflected from the bars as function of their depth and the work frequency.

Table 2: Numerically determined reflection amplitudes from bars located at different depths as function of the chosen work frequency.

Depth	**Amplitude**		
	$f_1 = 1GHz$	$f_2 = 1.6GHz$	$f_3 = 2GHz$
5cm	-303	-294	-192
10cm	-145	-201	-74
20cm	-98	-87	-52

The amplitudes given in Table 2 are next used to calculate the geometric attenuation parameter α for each work frequency. The obtained results are as follows: $\alpha_1 = 0.32$ for the frequency f_1; $\alpha_2 = 0.30$ for the frequency f_2 and $\alpha_3 = 0.27$ for the frequency f_3.

From Table 2, one can see that the amplitudes decrease with frequency. The geometric attenuation decreases also with frequency. As R_H decreases in its turn with frequency, no conclusion can be made regarding the effect of frequency on horizontal resolution limit before calculating the resolution from Eq. (4). Table 3 gives the obtained values of R_H and Δh as function of the work frequency and depth.

Table 3: Calculated footprint radius R_H and horizontal resolution Δh versus the depth for a given work frequency.

Depth	$f_1 = 1GHz$		$f_2 = 1.6GHz$		$f_3 = 2GHz$	
	R_H	Δh	R_H	Δh	R_H	Δh
5cm	0.055	0.042	0.044	0.034	0.039	0.031
10cm	0.078	0.059	0.062	0.048	0.055	0.044
20cm	0.111	0.084	0.087	0.087	0.078	0.062

From Table 3, it is seen that the horizontal resolution limit decreases at a given depth with the work frequency. It is seen also that the horizontal resolution limit is largely affected by depth. It almost doubles when the depth passes from $5cm$ to $20cm$.

To test further the horizontal resolution limit as predicted by Eq. (4), examination of the aspect of the obtained radargram was performed. Simulations are conducted by varying the horizontal interval distance separating the steel bars in a row placed at a given depth. Fig. 8 gives the radargram in the case of $f_3 = 2GHz$ for the interval distance $5cm$ and depth $d = 20cm$.

It is clear in Fig.8 that interference has occurred and detection of the two bars is impossible. Only one hyperbola trace appears in the radargram. This observation is conform with the horizontal resolution limit which is in this case, as given in Table 3, equal to $6.2cm$.

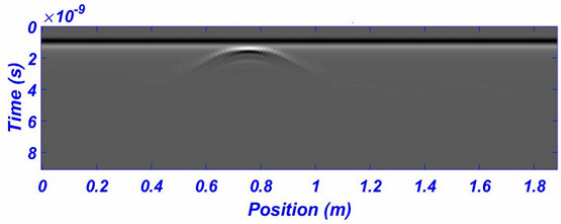

Fig. 8. B-scan radargram obtained with $f_3 = 2GHz$ for the concrete structure having two steel bars placed horizontally at $20cm$ of depth and separated by $5cm$.

Considering the work frequency $f_2 = 1.6GHz$ and varying the interval distance separating two adjacent steel bars that are placed in a row at a given depth, Table 4 gives the conclusion in terms of detectability, or presence of interference. This was determined after studying each simulated radargram.

Table 4 corroborates the results given on Table 3. No detection is possible when the horizontal distance separating two adjacent bars is lesser than the horizontal resolution limit predicted by Eq. (4).

Table 4: Qualitative evaluation of detectability made by direct observation on the obtained radargram for $f_2 = 1.6GHz$, the bars are placed horizontally with given depth and distance.

Depth	Horizontal distance (m)	detectability
$5cm$	0.015	No
	0.025	Interference
	0.034	Yes
$10cm$	0.025	No
	0.035	Interference
	0.048	Yes
$20cm$	0.055	No
	0.065	Interference
	0.087	Yes

3.2 Vertical resolution

As shown by Eq. (1), the vertical resolution Δv depends on the width of the pulse emitted by the GPR antenna as well as the wave velocity in the host medium. The pulse width can be estimated from the work frequency to be roughly $\tau_p = 1/f$. This gives for the vertical resolution the value $\Delta v = \lambda/2$. To test numerically this theoretical resolution limit, numerical simulations have been conducted with the work frequency $f_2 = 1.6GHz$ by varying the vertical distance separating two adjacent steel bars. Qualitative evaluation of detectability was performed then through studying the obtained radargram. The conclusions are reported in Table 5. Comparison is also done with the vertical resolution predicted by means of Eq. (1). This latter is given in the last column.

Table 5: Qualitative evaluation of detectability made by direct observation on the simulated radargram for $f_2 = 1.6GHz$, the bars are placed vertically with given depth and distance.

Depth	Vertical distance (m)	Detectability	$\Delta v = \lambda/2$
$5cm$	0.019	No	0.038
	0.025	Interference	0.038
	0.038	Yes	0.038
$10cm$	0.035	No	0.038
	0.045	Interference	0.038
	0.062	Yes	0.038
$20cm$	0.065	No	0.038
	0.085	Interference	0.038
	0.112	Yes	0.038

From Table 5, it is seen that $\Delta v = \lambda/2$ predicts the observed vertical resolution limit only for the depth of $5cm$. The numerically determined vertical resolution limit is found to be larger than that predicted by Eq. (1) for depths exceeding $10cm$. This is because of shadowing effect induced by the upper bar, which impedes the emitted signal to hit the lower bar with significant intensity such that it could provoke a reflected signal that can be sensed. The theoretical formula as given in Eq. (1) does not take into account this shadowing effect which is of huge importance in practice. Its predictions underestimate the real vertical resolution.

4 Conclusions

Considering concrete structures reinforced with steel bars, numerical simulations which were oriented towards evaluating qualitatively horizontal and vertical resolutions have been performed in this work. This was achieved by means of GprMax2D software. Comparison was made with two conventional formulas that were introduced in the literature to estimate GPR resolution in both directions. It was found that the equation predicting the horizontal resolution gives accurate results with respect to the observations made. This former should then be corrected by taking into account geometric attenuation as mentioned in the present work. However, the theoretical predictions regarding the vertical resolution hold only for shallow depths. Large errors are observed when using the formula of vertical resolution for deep targets. So, in practice detection will only be possible for bars that are separated vertically with a minimal distance that is larger than that predicted by the theoretical formula. This observation may be understood if one considers the shadowing effect which occurs in reality when two bars are placed vertically one above each other.

References

1. A. Benedetto, L. Pajewski, *Civil engineering applications of ground penetrating radar* (Springer , 2015)
2. T. Bachiri, G. Alsharahi, A. Khamlichi, M. Bezzazi, A. Faize, Int. J. of Emerg. Trends in Eng. Res. **8**, 5 (2020)
3. B. Riveiro, M. Solla, *Non-destructive techniques for the evaluation of structures and infrastructure* (CRC Press, 2016)
4. T. Bachiri, G. Alsharahi, A. Khamlichi, M. Bezzazi, A. Faize, *Ground penetrating radar data acquisition to detect imbalances and underground pipes* (in Lecture Notes in Electrical Engineering book series, volume 745, Springer, 2021)
5. F.A. Catalan, R.S. Pagtalunan, E.A. Malit, K.A.S. Chavez, L.K.S. Tolentino, Int. J. of Emerging Trends in Engineering Research **8**, 10 (2020)
6. A.P. Annan, *Ground penetrating radar principles, procedures and applications* (Sensors and software Incorporated, Ontario, Canada, 2003)
7. C.W. Chang, C.H. Lin, H.S. Lien, Construction and Building Materials **23**, 2 (2009)
8. H.L. Cimadevila, *Prospección geofísica de alta resolución mediante geo-radar; aplicación a obras*

civiles (Doctoral dissertation, Universidad Complutense de Madrid, 1994)

9. Z. Mechbal, A. Khamlichi, MATEC Web of Conferences **16** (2014)
10. F. Tosti, C. Ferrante, Surveys in Geophysics **41**, 3 (2020)
11. J. Lachowicz, M. Rucka, Diagnostyka **16** (2015)
12. F.I. Rial, M. Pereira, H. Lorenzo, P. Arias, A. Novo, Journal of Applied geophysics **67**, 4 (2009)
13. A. Giannopoulos, Construction and building materials **19**, 10 (2005)
14. V. Pérez-Gracia, R. González-Drigo, D. Di Capua, NDT & E International **41**, 8 (2008)
15. T. Ziani, D. Teguig, M.A. Takkouche, X. Dérobert, M. Benslama, *GPR modelling applied to vertical and horizontal resolution of buried objects* (In proceedings of International Conference on Electromagnetics in Advanced Applications, IEEE, 2011).
16. T. Bachiri, M. Hamdaoui, G. Alsharahi, M. Bezzazi, A. Faize, MATEC Web of Conferences **360**, (2022)